Heparan sulfate proteoglycans mediate internalization and propagation of specific proteopathic seeds

Brandon B. Holmes[a], Sarah L. DeVos[a], Najla Kfoury[a], Mei Li[b], Rachel Jacks[a], Kiran Yanamandra[a], Mohand O. Ouidja[c], Frances M. Brodsky[d], Jayne Marasa[e], Devika P. Bagchi[a], Paul T. Kotzbauer[a], Timothy M. Miller[a], Dulce Papy-Garcia[c], and Marc I. Diamond[a,1]

[a]Department of Neurology, Washington University School of Medicine, St. Louis, MO 63110; [b]Vision Science Core, University of California, Berkeley, School of Optometry, Berkeley, CA 94720; [c]Laboratoire Croissance, Réparation et Régénération Tissulaires, Centre National de la Recherche Scientifique FRE24-12, Université Paris XII-Val de Marne, 94010 Créteil, France; [d]Departments of Bioengineering and Therapeutic Sciences, G. W. Hooper Foundation, University of California, San Francisco, CA 94143; [e]Bridging Research with Imaging, Genomics, and High-Throughput Technologies Institute, Washington University School of Medicine, St. Louis, MO 63110

Edited by Gregory A. Petsko, Brandeis University, Waltham, MA, and approved June 28, 2013 (received for review January 23, 2013)

Recent experimental evidence suggests that transcellular propagation of fibrillar protein aggregates drives the progression of neurodegenerative diseases in a prion-like manner. This phenomenon is now well described in cell and animal models and involves the release of protein aggregates into the extracellular space. Free aggregates then enter neighboring cells to seed further fibrillization. The mechanism by which aggregated extracellular proteins such as tau and α-synuclein bind and enter cells to trigger intracellular fibril formation is unknown. Prior work indicates that prion protein aggregates bind heparan sulfate proteoglycans (HSPGs) on the cell surface to transmit pathologic processes. Here, we find that tau fibril uptake also occurs via HSPG binding. This is blocked in cultured cells and primary neurons by heparin, chlorate, heparinase, and genetic knockdown of a key HSPG synthetic enzyme, *Ext1*. Interference with tau binding to HSPGs prevents recombinant tau fibrils from inducing intracellular aggregation and blocks transcellular aggregate propagation. In vivo, a heparin mimetic, F6, blocks neuronal uptake of stereotactically injected tau fibrils. Finally, uptake and seeding by α-synuclein fibrils, but not huntingtin fibrils, occurs by the same mechanism as tau. This work suggests a unifying mechanism of cell uptake and propagation for tauopathy and synucleinopathy.

neurodegeneration | Alzheimer's disease | prion-like mechanisms | macropinocytosis

Alzheimer's disease (AD), frontotemporal dementia, and other tauopathies feature conversion of soluble, native tau protein into filamentous aggregates. In AD, tau pathology and its associated neural atrophy do not distribute randomly throughout the brain, but progress in association with neural networks (1–4), implying a role for connectivity and the transcellular movement of a pathological agent (1, 2, 4, 5). Prior studies by our laboratory and others have demonstrated that internalized tau aggregates can trigger fibrillization of native tau protein (6–11). We have previously observed that tau aggregates propagate the misfolded state among cells in culture via release of fibrils into the extracellular space. These aggregates trigger further fibrillization by direct protein–protein contact with native tau in the recipient cells (12). Thus, fibrillar tau appears to spread pathologic processes by mechanisms fundamentally similar to prion pathogenesis. Although the phenomenology is now well described, the basic mechanisms that mediate transcellular propagation of tau aggregation remain unknown, including the mechanism of aggregate uptake to seed intracellular fibrillization. Infectious prion protein is known to bind heparan sulfate proteoglycans (HSPGs) on the cell surface, a requirement for propagation of the pathological conformation (13, 14). This study elucidates a mechanism whereby tau aggregates bind HSPGs to stimulate cell uptake via macropinocytosis and seed further aggregation. Further, we find that HSPGs also mediate uptake and seeding of α-synuclein fibrils, but not huntingtin fibrils, consistent with a unifying mechanism for two major classes of neurodegenerative disease.

Results

Tau Fibrils Enter Cells via Macropinocytosis. The precise mechanism for tau aggregate entry into cells is unknown. We have previously studied the cellular uptake of tau that comprises the repeat domain (RD), the aggregation-prone core of the protein. RD fibrils, but not monomer, are readily internalized into murine C17.2 neural precursor cells by fluid-phase endocytosis (6). We have now confirmed that this active process does not require clathrin or caveolin-mediated endocytosis (*SI Text* and Figs. S1 and S2). Several mechanisms can account for fluid-phase endocytosis, including macropinocytosis, which is characterized by actin-driven membrane ruffling, internalization of extracellular fluids, and formation of large intracellular vacuoles (0.5–10 μM). Under certain circumstances, a variety of particles, including bacteria and viruses, can induce macropinocytosis for cell entry (15). We thus tested the role of macropinocytosis in tau fibril internalization. First, we covalently labeled tau RD fibrils with Alexa Fluor 488 (i.e., RD-488) and applied them to the media of C17.2 cells. We subsequently stained the cells with rhodamine-tagged phalloidin to label filamentous actin, which surrounded large tau inclusions (Fig. 1*A*). This is typical of macropinosomes, which require actin rearrangement to create lamellipodia-like membrane protrusions. By using EM, we investigated the ultrastructure of cells treated with tau RD fibrils (Fig. 1*B*). After 1 h

Significance

Prion-like propagation of proteopathic seeds may underlie the progression of neurodegenerative diseases, including the tauopathies and synucleinopathies. Aggregate entry into the cell is a crucial step in transcellular propagation. We used chemical, enzymatic, and genetic methods to identify heparan sulfate proteoglycans as critical mediators of tau aggregate binding and uptake, and subsequent seeding of normal intracellular tau. This pathway mediates aggregate uptake in cultured cells, primary neurons, and brain. α-Synuclein fibrils use the same entry mechanism to seed intracellular aggregation, whereas huntingtin fibrils do not. This establishes the molecular basis for a key step in aggregate propagation.

Author contributions: B.B.H., N.K., M.L., R.J., and M.I.D. designed research; B.B.H., S.L.D., N.K., M.L., R.J., and K.Y. performed research; B.B.H., M.O.O., F.M.B., J.M., D.P.B., P.T.K., T.M.M., and D.P.-G. contributed new reagents/analytic tools; B.B.H. and M.I.D. analyzed data; and B.B.H. and M.I.D. wrote the paper.

The authors declare no conflict of interest.

This article is a PNAS Direct Submission.

[1]To whom correspondence should be addressed. E-mail: diamondm@neuro.wustl.edu.

This article contains supporting information online at www.pnas.org/lookup/suppl/doi:10.1073/pnas.1301440110/-/DCSupplemental.

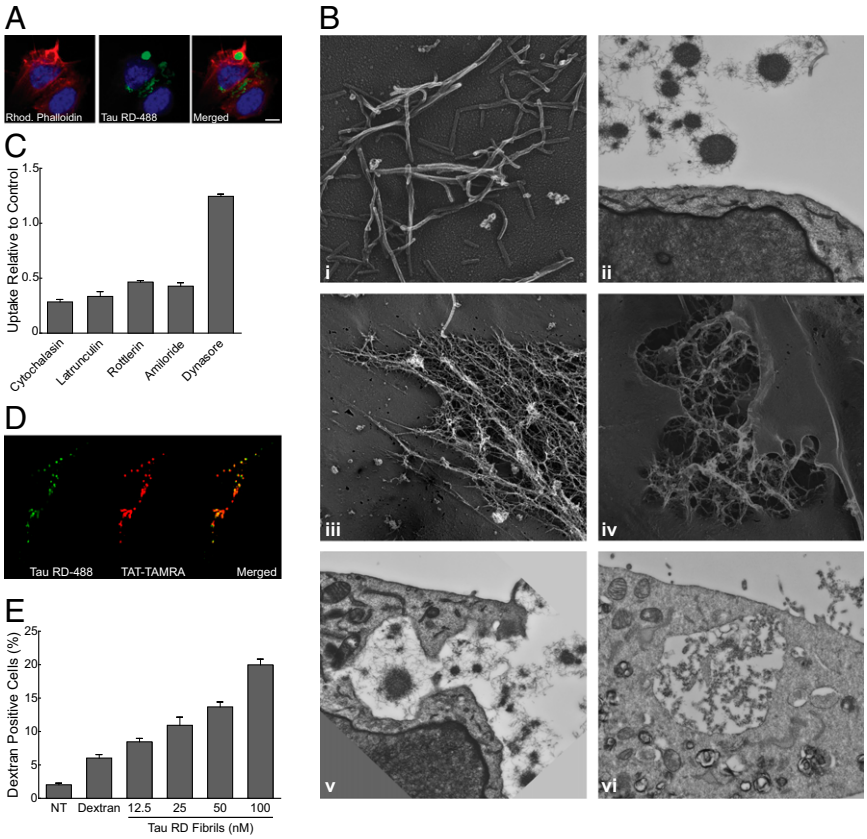

Fig. 1. Tau RD fibril internalization is mediated by macropinocytosis. (*A*) Internalized tau RD fibrils are associated with filamentous actin as demonstrated by colocalization with rhodamine-phalloidin. (Scale bar: 10 μm.) (*B*) EM ultrastructure of tau fibrils and their association with the plasma membrane. (*i*) Scanning EM image of tau RD fibrils. (*ii*) Tau RD fibrils near the plasma membrane of a C17.2 cell. (*iii*) Tau RD fibrils adherent to the membrane of a cell. (*iv*) Top-down view of tau fibrils engulfed in lamellipodia-like membrane protrusion. (*v*) Cross-sectional view of tau fibrils surrounded by lamellipodia-like membrane protrusion. (*vi*) Large tau fibril-containing vesicle within a cell. (*C*) Inhibition of macropinocytosis reduces tau fibril uptake as measured by flow cytometry after exposure of cells to tau RD-488 fibrils for 90 min. Data are expressed relative to the untreated control group. A total of 25,000 cells were analyzed per group in each experiment, and the graph represents the average of two independent experiments. (*D*) Tau fibrils colocalize with macropinosome marker TAT-TAMRA. (*E*) Tau RD fibrils stimulate fluid-phase endocytosis. A total of 100 μg/mL of dextran-fluorescein was applied to cells in the presence of increasing concentrations of unlabeled tau RD fibrils for 90 min before analysis by automated microscopy. NT, not treated.

of fibril treatment, we observed tau RD fibrils adherent to the plasma membrane, and, in many instances, we observed engulfment of fibrils by lamellipodia-like membrane protrusions. Further, internalized fibrils were contained within large membrane-bound vacuoles that often exceeded 5 μM in diameter, which are significantly larger than other endocytic vesicles, and consistent with macropinosomes.

To further characterize the mechanism of entry, we tested macropinosome inhibitors by using flow cytometry to monitor uptake of RD-488 fibrils (Fig. 1*C*). Cytochalasin D (1 μM) and latrunculin (1 μM), inhibitors of actin polymerization, markedly decreased uptake of tau RD-488 fibrils. Similarly, 5-*N*-ethyl-*N*-isopropyl-amiloride (1 mM), an inhibitor of Na^+/H^+ exchange, and rottlerin (30 μM), an inhibitor of PKC kinase, strongly diminished fibril uptake, also consistent with macropinocytosis. Tau fibril uptake was independent of dynamin 1, as the inhibitor Dynasore (80 μM) did not reduce tau internalization.

Next we determined whether tau fibrils would colocalize with the HIV-derived transactivator of transcription (TAT) peptide, which is known to enter cells via macropinocytosis (16–19). We used TAT fused to a fluorescent dye, carboxytetramethylrhodamine (TAMRA), as a marker of macropinosomes. We coadministered 5 μM TAT-TAMRA and 50 nM of tau RD-488 fibrils to C17.2 cells for 90 min before confocal microscopy. TAT and tau RD fibrils showed nearly identical localization in puncta throughout the cells (Fig. 1*D*). We excluded the possibility that tau fibrils directly bind the TAT peptide (which would not be predicted, based on a similarly positive charge) by using surface plasmon resonance (Fig. S3). Finally, we tested whether tau fibrils directly stimulate macropinocytosis. We added increasing concentrations of unlabeled tau RD fibrils to C17.2 cells in the presence of dextran-fluorescein to mark fluid-phase endocytosis. Coadministration of fibrils dose-dependently increased dextran uptake from 6% to 20% of cells (Fig. 1*E*). Thus, extracellular tau aggregates directly stimulate macropinocytosis to trigger their own uptake.

HSPGs Mediate Tau Fibril Binding and Uptake. Tau and TAT contain heparin-binding domains, and it is established that TAT enters cells via HSPG-mediated macropinocytosis (20–25). Given the extensive colocalization between tau fibrils and TAT after endocytosis, we hypothesized that HSPGs might also mediate cellular binding and internalization of tau aggregates. HSPGs are transmembrane and lipid-anchored cell surface receptors that interact with a variety of ligands. They are extensively sulfated, a crucial posttranslational modification. These sulfated moieties permit electrostatic interactions between the sugar polymers and short basic amino acid stretches in heparin-binding proteins.

To determine if tau fibrils and HSPGs colocalize, we treated C17.2 cells with 50 nM tau RD-488 fibrils for 60 min, removed

extracellular fibrils by using trypsin, and allowed the cells to recover before immunostaining for HSPGs. We found that the HSPGs enveloped the RD-488 puncta (Fig. 2*A*), consistent with the tau fibrils within macropinosomes that we had observed by EM. We next investigated whether HSPGs mediate binding of tau fibrils to the cell surface. We incubated C17.2 cells with RD-488 fibrils at 4 °C in the presence or absence of HSPG inhibitors and imaged cells by using confocal microscopy. At this restrictive temperature tau fibrils are not internalized, but instead adhere to the cell membrane. We then tested two chemical inhibitors of tau/HSPG interactions. Sodium chlorate, a metabolic inhibitor, prevents proper sulfation of HSPGs. Conversely, heparin, a glycosaminoglycan, competitively inhibits tau binding to HSPGs. Both compounds dose-dependently blocked tau RD binding to the cell surface, as determined by confocal microscopy (Fig. 2*B*) and flow cytometry (Fig. 2 *C* and *D*). The effective concentrations were consistent with those reported previously by others (14, 26). Taken together, this work suggests that HSPGs mediate tau fibril binding to the cell surface.

We further examined the role of HSPGs for tau fibril internalization by using automated high-content microscopy (IN Cell Analyzer 1000; GE Healthcare). This method permits quantification of the percentage of cells within a population that are positive for labeled tau aggregates, and the average number of tau aggregates per cell (among positive cells). This latter quantification allows determination of the "tau aggregate burden" in tau-positive cells. We treated C17.2 cells with chlorate or heparin before exposure to 50 nM RD-488 fibrils for 3 h. After a 5-min trypsin treatment, cells were replated and imaged by confocal or automated microscopy (Fig. 3 *A*–*D*). Heparin and chlorate dose-dependently decreased the internalization of tau fibrils within the same concentration ranges that blocked cell surface binding. They also reduced the average number of tau aggregates per cell, demonstrating that inhibition of tau binding to HSPGs decreases the subsequent total tau burden in aggregate-positive cells (Fig. 3 *B* and *C*).

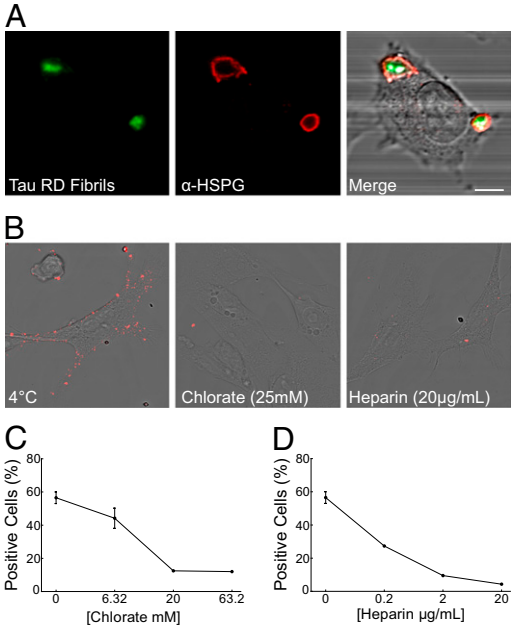

Fig. 2. HSPGs mediate binding of tau RD fibrils to C17.2 cells. (*A*) Tau RD-488 fibrils colocalize with anti-HSPG antibody (10E4). (Scale bar: 10 μm.) (*B*) At 4 °C, tau RD-546 fibrils bind to the plasma membrane but are not internalized, a process that is inhibited by pretreatment with heparin and chlorate. HSPG inhibition abolishes the association between tau RD fibrils and C17.2 cells observed by confocal microscopy. (*C* and *D*) Flow cytometry quantification of tau fibril binding to the cell membrane in the presence of chlorate or heparin. Cells were treated with 50 nM tau RD-488 fibrils at 4 °C for 1 h. A total of 25,000 cells were analyzed for each condition, which was run in triplicate. Error bars show SEM.

Next we used enzymatic modification of HSPGs to investigate their role in fibril uptake. We pretreated C17.2 cells with increasing concentrations of heparinase III or chondroitinase AC to specifically degrade cell surface heparan or chondroitin sulfates, respectively. Heparinase III dose-dependently decreased the percentage of tau aggregate-positive cells and total aggregates per cell, whereas chondroitinase AC had no effect alone or in combination with heparinase III (Fig. 3*D* and Fig. S4). Thus, HSPGs, and not chondroitin sulfates, are critical for tau fibril uptake. To rule out nonspecific effects, we treated cells for 90 min with 25 μg/mL transferrin, a substrate of clathrin-mediated endocytosis, covalently labeled with Alexa Fluor-488 (i.e., Tfn-488). Heparin, chlorate, heparinase III, and chondroitinase AC had no effect on Tfn-488 uptake (Fig. 3*E*). Thus, tau RD fibril binding to HSPGs is critical for uptake by macropinocytosis in C17.2 cells.

Full-Length Tau Requires HSPGs to Enter Neurons. Tau RD is commonly used because of its efficient fibril formation. However, we wanted to determine whether full-length (FL) tau fibril internalization is also mediated by HSPGs. We applied 50 nM FL tau-488 fibrils to C17.2 cells in the presence or absence of chlorate and heparin. FL tau fibril uptake was approximately two- to fourfold more sensitive to HSPG inhibition than RD fibrils (Fig. 4 *A* and *B*). Thus, FL tau aggregates also require HSPGs for cellular internalization.

To test the involvement of HSPGs in primary hippocampal neurons, we knocked down a key HSPG biosynthesis enzyme, *Ext1*, before exposure to FL tau aggregates. Although critical to synthesis of HSPGs, *Ext1* is not rate-limiting in their production (27). Cells deficient in *Ext1* cannot produce HSPGs, although they can produce other glycosaminoglycans (28). We first identified potent shRNAs against *Ext1* by screening five different constructs in C17.2 cells by quantitative real-time (RT)-PCR and selecting a lentivirus that achieved ∼90% *Ext1* knockdown (Fig. 4*C*). Next, we transduced primary neurons and used flow cytometry to quantify aggregate uptake based on mean cell fluorescence intensity. We observed a 43% reduction of 50 nM FL tau fibril uptake relative to neurons treated with control luciferase shRNA (Fig. 4*D*). *Ext1* knockdown did not affect Tfn-488 uptake (Fig. 4*E*), confirming that inhibition of tau fibril uptake in neurons is specific to the HSPG pathway, as in other cells. In summary, pharmacological, enzymatic, and genetic manipulations implicate HSPGs as key receptors for recombinant FL tau and RD fibrils in neural cell lines and primary neurons alike.

HSPG Inhibition Blocks Aggregate Propagation. Although HSPGs mediate virtually all detectable tau uptake, it remained possible that other modes of cell entry could permit propagation of aggregation into cells. Thus, we used previously developed methods to test whether blockade of HSPGs would inhibit seeded aggregation and transcellular propagation of RD fibrils. We have previously found that fusion of RD containing a disease-associated mutation (ΔK280) to CFP or YFP [i.e., RD(ΔK)CFP/YFP] allows quantification of intracellular aggregation based on FRET (12). Incubation of HEK293 cells expressing tau RD-CFP/YFP with 50 nM tau RD fibrils increased intracellular aggregation as expected. However, pretreatment with heparin or heparinase III decreased induction of intracellular aggregation by recombinant fibrils (Fig. 5*A*) without affecting intrinsic intracellular aggregation (Fig. 5*B*).

No effective assay exists to measure transcellular propagation of tau aggregates in primary neurons. Thus, to test the role of

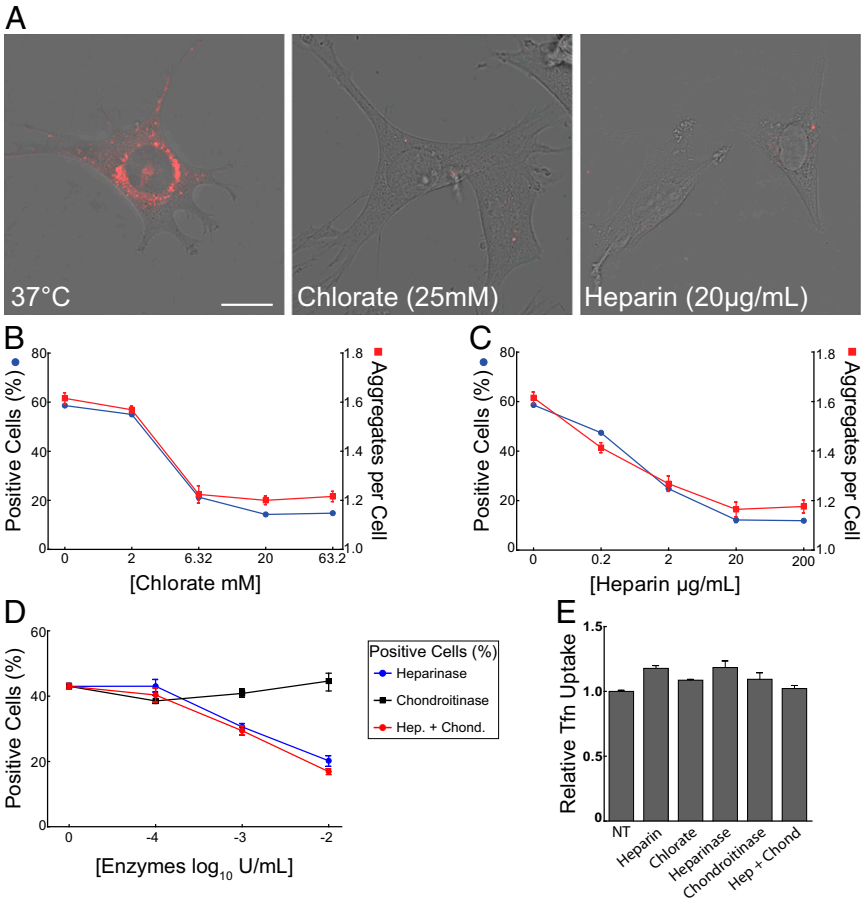

Fig. 3. HSPGs mediate tau RD fibril uptake. (*A*) At 37 °C, tau RD-546 fibrils are internalized by the cell, a process that is inhibited by chlorate and heparin. (Scale bar: 20 μm.) (*B* and *C*) Automated microscopy analysis of tau fibril internalization in the presence of chlorate or heparin. Cells were treated with 50 nM tau RD-488 fibrils and chlorate or heparin at 37 °C for 3 h and trypsinized before imaging. The left *y*-axis (blue) depicts percentage of positive cells and the right *y*-axis (red) depicts the average number of tau aggregates per cell. Approximately 40,000 cells were analyzed for each condition, run in quadruplicate. (*D*) Percent cells positive for tau fibril internalization in the presence of heparinase III or chondroitinase AC as measured by automated microscopy analysis. Approximately 40,000 cells were analyzed for each condition, run in duplicate. (*E*) HSPG inhibition does not affect clathrin-mediated transferrin endocytosis. Internalization of Tfn-488 (25 μg/mL) was unaltered in the presence of chlorate (63.2 mM), heparin (200 μg/mL), heparinase III, or chondroitinase AC (10^2 IU/mL) as measured by flow cytometry mean fluorescence intensity. A total of 25,000 cells were analyzed for each condition in duplicate. The nontreated group (NT) received no inhibitor, and data reflect uptake relative to this group. (Error bars: *B*, *C*, and *E*, SEM; *D*, range.)

HSPGs in this process, we used a HEK293 cell coculture assay in which donor cells express untagged tau RD that contains two disease-associated mutations, P301L and V337M [termed RD (LM)], that greatly increases its intrinsic aggregation propensity. RD(LM) aggregates are released by the donor cells into the media, taken up by aggregation-sensor cells expressing RD(ΔK)-CFP/YFP, and nucleate further tau aggregation, as measured by FRET (12). We cultured donor cells expressing tau RD(LM) with an equal number of acceptor cells expressing RD(ΔK)-CFP/YFP. After 48 h, we observed a significant increase in FRET, indicating propagation of aggregation from donor to acceptor cells. Heparin titration and heparinase III pretreatment blocked the induced aggregation, demonstrating inhibition of transcellular propagation (Fig. 5*C*). Thus, HSPGs mediate propagation of aggregation from the outside to the inside of the cell as well as between cells.

HSPGs Are Required for FL Tau Fibril Entry in Vivo. We next investigated the role of HSPGs as a receptor for tau fibrils in vivo. Heparin has strong anticoagulant properties that preclude its use within mouse brain. On the contrary, heparin mimetics that do not promote bleeding are promising therapeutic agents for wound healing and for blocking prion infectivity (29, 30). We screened a selection of synthetic heparin mimetics for activity in blocking tau aggregate uptake, and selected F6 for its potency and lack of anticoagulation activity (Fig. S5). We first tested F6 as a potential inhibitor of tau fibril internalization, seeded aggregation, and transcellular propagation in cell culture. We used polymeric dextran (PD), a nonsulfated heparin mimetic, as a negative control (Fig. S5). Based on automated microscopy analysis of C17.2 cells, F6 potently inhibited recombinant tau fibril internalization, whereas PD had no effect (Fig. 6*A*). In HEK293 cells, F6 also blocked seeded aggregation and transcellular propagation with an IC_{50} similar to that of heparin (Fig. 6 *B* and *C*), and it had no effect on cell-autonomous tau aggregation (Fig. 6*D*).

To test the effect of blocking tau fibril binding to HSPGs in vivo, we coinjected 472 ng of FL tau-488 fibrils with 1 μg of F6 or PD into the cortex of 5-mo-old WT mice (Fig. 7*A*). After 48 h, mice were killed and cortical neurons in brain sections were identified by staining with anti-NeuN antibody. In mice coinjected with tau fibrils and PD, we observed a large number of tau fibril-positive neurons. All exhibited punctate morphology similar to our cell culture model. In mice coinjected with tau fibrils and F6, only a small fraction of neurons scored positive for tau aggregates, indicating that F6 blocked neuronal uptake (Fig. 7*B*).

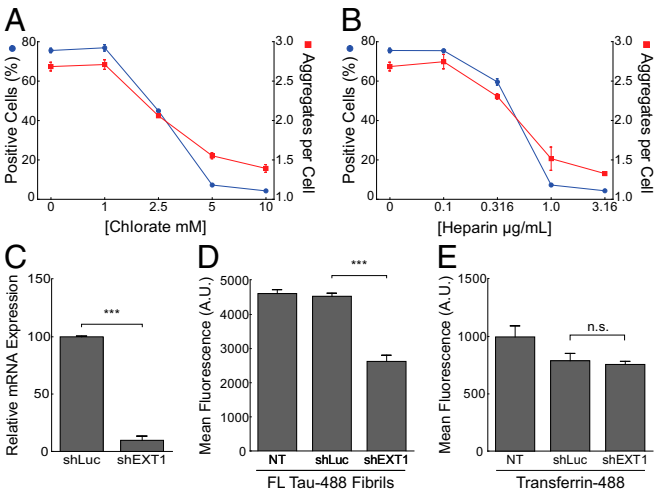

Fig. 4. HSPGs mediate internalization of FL tau fibrils in C17.2 cells and primary hippocampal neurons. (*A* and *B*) Automated microscopy analysis of FL tau-488 fibril internalization into C17.2 cells in the presence of chlorate or heparin. Cells were treated with 50 nM FL tau-488 fibrils at 37 °C for 3 h and trypsinized before imaging. Approximately 40,000 cells were analyzed for each condition and run in quadruplicate. The left *y*-axis (blue) depicts percentage of positive cells and the right *y* axis (red) depicts the average number of tau aggregates per cell. (*C*) Lentivirus encoding *Ext1* shRNA reduces *Ext1* transcript in C17.2 cells by quantitative PCR relative to GAPDH ($n = 3$). (*D*) Knockdown of murine *Ext1* by shRNA, but not *luciferase* shRNA, reduces the internalization of FL tau-488 fibrils into primary hippocampal neurons by mean fluorescence intensity measurements. The nontreated (NT) group received no shRNA ($n = 9$). Error bars show SEM. (*E*) Knockdown of murine *Ext1* by shRNA does not reduce Tfn-488 internalization into primary hippocampal neurons ($n = 4$, error bars show SEM; $^{***}P < 0.001$ by one-way ANOVA).

To rule out the possibility that F6 inhibited neuronal tau fibril entry as a result of cellular toxicity or other off-target effects, we injected 5 μg of Tfn-488 and PD or F6 in conjunction with FL tau fibrils labeled with Alexa Fluor-647. In mice receiving PD treatment, neurons near the injection site scored positive for tau fibrils and Tfn-488, indicating efficient uptake (Fig. 7*C* and Movie S1). However, in mice receiving F6 treatment, the majority of neurons had only internalized Tfn-488 (Fig. 7*D*). Image analysis (ImageJ; National Institutes of Health) indicated 64% of neurons were positive for tau fibrils when coinjected with PD, whereas only 30% were positive when coinjected with F6 (Fig. 7*E*). Similarly, F6 significantly reduced the mean fluorescence intensity for tau fibrils in neurons per animal by 50%, but not the mean fluorescence intensity of transferrin (Fig. 7 *F* and *G*). Thus, FL tau fibril uptake into neurons in vivo also requires binding to HSPGs.

HSPGs Mediate Internalization of α-Synuclein but Not Huntingtin. In addition to tau, α-synuclein and huntingtin accumulate in fibrillar aggregates and cause progressive neurodegeneration. Other studies have documented cellular uptake of these aggregated proteins, even though their specific mechanism of entry is unknown (31–33). We thus determined whether HSPGs mediate their cellular uptake and seeding activities. We began by testing whether α-synuclein and Htt(Q50) fibrils would colocalize with HSPGs. α-Synuclein monomer was purified from bacteria, allowed to fibrillize, and covalently labeled with Alexa Fluor-488. Htt(Q50) exon 1 monomer was prepared by solid-state synthesis, incorporating a fluorescein tag at the amino terminus. The Htt (Q50) peptide was allowed to fibrillize in solution. We then exposed C17.2 cells to these fibrils, followed by immunostaining for HSPGs. Consistent with previous reports (31–34), aggregates of both proteins were readily internalized into cells: α-synuclein in multiple small puncta, Htt(Q50) in a single perinuclear inclusion. Notably, α-synuclein colocalized with HSPGs whereas Htt(Q50) did not (Fig. 8 *A* and *B*).

To further test modes of uptake, we exposed C17.2 cells simultaneously to tau (labeled with Alexa Fluor-647), synuclein (labeled with Alexa Fluor-488), or Htt(Q50) (tagged with fluorescein), along with TAT-TAMRA. This combination of fluorescent labels allows simultaneous imaging of each protein by using confocal microscopy. We observed clear colocalization of tau, α-synuclein, and TAT, whereas Htt(Q50) partitioned to a distinct subcompartment (Fig. 8 *C* and *D*).

To confirm the role of HSPGs in α-synuclein uptake, we treated C17.2 cells with α-synuclein-488 fibrils or fluorescein-Htt (Q50) in the presence or absence of chlorate and heparin to block binding to HSPGs. Each compound dose-dependently inhibited internalization of α-synuclein fibrils, as measured by automated microscopy analysis (Fig. 8*E*); however, they had no effect on Htt(Q50) fibril uptake (Fig. 8*F*). Heparin likewise blocked the seeded aggregation of α-synuclein-CFP/YFP fusion proteins in a FRET assay that monitors endogenous α-synuclein fibrillization (Fig. 8*G*), whereas it had no effect on Htt(Q50) seeding of Htt(Q25)-CFP/YFP (Fig. 8*H*) (35). Taken together, these data indicate that tau and α-synuclein use a similar mechanism for uptake based on binding HSPGs, whereas Htt exon 1 fibril uptake is distinct.

Discussion

This study defines the principle mechanism governing cell uptake of tau aggregates to seed intracellular fibrillization. Aggregated tau enters cells via macropinocytosis, an actin-dependent process that allows macromolecular structures into the cell. Internalized tau fibrils colocalize almost perfectly with labeled TAT peptide, suggesting the involvement of HSPGs in its uptake. We confirmed the role of HSPGs by using pharmacologic and genetic studies. The results indicated that tau binding and internalization

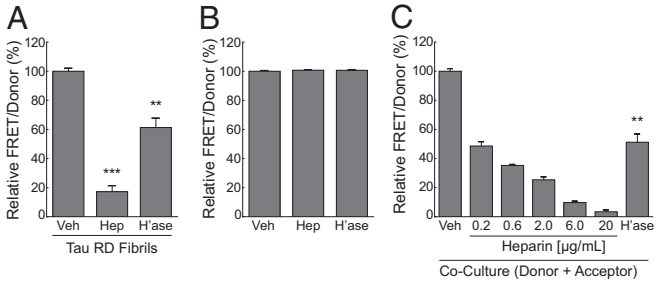

Fig. 5. Inhibition of HSPGs blocks seeded aggregation and transcellular propagation of tau aggregation. (*A*) Heparin (Hep) and heparinase (h'ase) inhibit intracellular seeding by recombinant tau RD fibrils in a cell-based FRET assay. HEK293 cells cotransfected with tau RD(ΔK)-CFP/YFP were pretreated with heparinase (0.01 IU/mL) for 3 h before treatment with tau fibrils or treated with tau RD fibrils plus vehicle or heparin (6 μg/mL) for 24 h before reading FRET measurements on a plate reader. The FRET signal is shown as a percentage relative to the vehicle treated group. (*B*) Neither heparin nor heparinase affect cell-autonomous tau aggregation. Cells expressing RD (ΔK)-CFP/YFP were treated with vehicle or heparin (6 μg/mL) for 24 h or heparinase (0.01 IU/mL) for 27 h. A value of 100% represents baseline aggregation signal for the vehicle-treated group. (*C*) Heparin and heparinase block transcellular propagation. HEK293 cells expressing RD(ΔK)-CFP/YFP were cocultured with an equivalent number of cells expressing tau RD(LM)-HA for 48 h to monitor transcellular propagation of tau protein misfolding. Heparin dose dependently inhibited transcellular aggregate propagation, as did 0.01IU/mL of heparinase. The FRET signal is shown as a percentage relative to the vehicle-treated group. Error bars show SEM from four biological replicates per experiment for heparin and from six biological replicates per experiment for heparinase ($^{***}P < 0.001$, $^{**}P < 0.01$, Student *t* test).

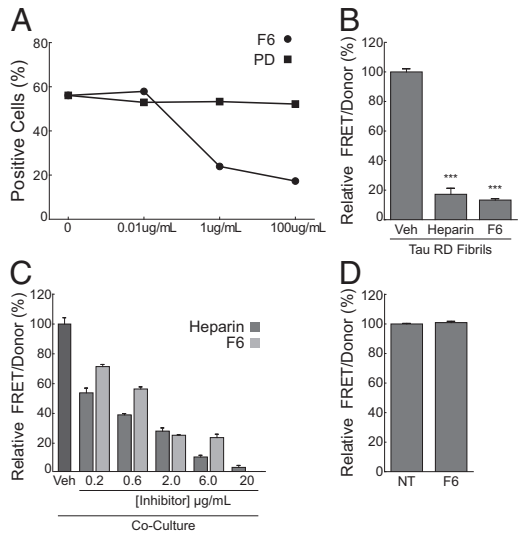

Fig. 6. Heparin mimetic F6 inhibits tau fibril uptake and induction of misfolding. (*A*) F6 inhibits tau RD fibril internalization into C17.2 cells whereas PD has no effect. Cells were treated with 50 nM tau RD-AF488 fibrils at 37 °C for 3 h and trypsinized before replating and imaging with automated microscopy. Approximately 40,000 cells were analyzed for each condition and run in quadruplicate. (*B*) F6 (6 μg/mL) and heparin (6 μg/mL) equivalently inhibit seeded aggregation in a FRET-based assay. (*C*) F6 and heparin each block transcellular propagation between cells expressing tau RD(LM) and cells expressing RD(ΔK)-CFP/YFP. (*B* and *C*) FRET signal is shown as a percentage relative to the vehicle treated group. (*D*) F6 does not inhibit cell-autonomous tau aggregation. A value of 100% represents baseline aggregation signal of the vehicle-treated group. Error bars show SEM from four biological replicates per experiment (***$P < 0.001$, Student *t* test).

into neurons are mediated by HSPGs in vitro and in vivo. Further, internalization by this pathway is required for extracellular fibrils to seed intracellular tau aggregation, and for transcellular propagation. α-Synuclein fibrils, but not Htt exon 1 fibrils, use a similar mechanism. We have thus defined HSPGs as a receptor for cell uptake of tau and α-synuclein, a critical step in prion-like propagation of aggregation.

We and others have previously suggested that tau aggregate propagation from cell to cell mediates the spread of neurodegeneration through the brain, and multiple studies have now confirmed the basic phenomenology. The mechanisms governing this process, especially the specific proteins and pathways required for these events, have been unclear. This work has thus helped clarify a key step in the propagation of pathologic conditions by determining that pathogenic tau aggregates use HSPGs to bind the cell surface. This actively stimulates macropinocytosis, which is required for propagation of aggregation between cells in culture and for uptake of aggregates in vivo.

Aggregate Uptake by Macropinocytosis. Based on pharmacologic studies and colocalization with fluid phase markers, macropinocytosis was previously suggested as the mechanism for cell uptake of SOD1 (36). Likewise, macropinocytosis and HSPGs have been previously implicated in prion protein uptake (14, 37). In this study, we investigated the molecular basis of uptake with a multifaceted approach. We initially used EM to directly image uptake events. This indicated that the cell internalizes tau fibrils via dynamic membrane rearrangement and forms large endocytic vesicles consistent with macropinosomes. Indeed, extracellular tau fibrils stimulated fluid-phase endocytosis in a dose-dependent fashion. We subsequently observed colocalization of aggregates with labeled TAT peptide, which is known to enter cells via macropinocytosis (17–19). Other mechanisms of cell uptake have been proposed for protein aggregates, including dynamin-dependent endocytosis (31, 38) and direct permeabilization of the cell membrane (35, 39), neither of which appear to contribute to tau aggregate uptake in our studies.

Aggregate propagation requires direct contact between the macropinosome-encapsulated seed and the cytosolic monomer. However, it remains unclear how a tau aggregate traverses the membrane barrier of a macropinosome. Of note, viruses and cell-penetrating peptides such as TAT exploit macropinosomes to enter the cytosol (17, 40, 41), also by unclear mechanisms. Macropinosomes are inherently leaky in comparison with other types of endosomes (42), which may allow contents to escape, and thus permit fibrils to seed aggregation in the cytosol. We hypothesize that fibrils may actually promote their own escape from the vesicular compartment based on destabilization of the lipid bilayer. This remains to be tested, but has been proposed as a property of tau oligomers (43).

HSPGs Mediate Tau Uptake. HSPGs participate in numerous cell surface interactions and serve as a primary receptor for macropinocytosis (19). Heparin-binding proteins interact with HSPGs on the cell surface, triggering internalization. In addition to our work with tau and α-synuclein, this mechanism has previously been demonstrated for infectious prion protein and Aβ monomer (14, 26). Binding to HSPGs requires a heparin/heparan sulfate-binding domain consisting of a stretch of positively charged lysines or arginines on the ligand. Prion protein, β-amyloid, tau, and α-synuclein all have putative heparin-binding domains (25, 44–46).

We have found a critical role for HSPGs in selectively binding and internalizing aggregated tau. We picked a tau aggregate concentration for our studies (50 nM monomer equivalent) that roughly approximates physiologic levels, based on our best estimates. Currently, it is impossible to quantify tau aggregate concentration in the brain interstitial fluid (ISF) of humans or tauopathy animal models. Our recent work used a microdialysis technique that measures only tau monomer in brain ISF. We estimated a concentration of ~250 ng/mL (~17 nM, assuming FL tau) in P301S human tau transgenic mice (47), but total ISF tau levels (including aggregates) may in fact be higher. In this study, we potently inhibited tau aggregate binding, uptake, and seeding of intracellular aggregation with multiple compounds specific to this pathway: heparinase III, an enzyme that degrades cell surface HSPGs; heparin, which blocks binding to HSPGs; and chlorate, a metabolic inhibitor of sulfation. We also tested this pathway by knockdown of *Ext1*, which is involved in elongation of heparan sulfate chains, and is critical to HSPG synthesis (28, 48). Genetic knockdown of *Ext1* has been used extensively in cell culture to probe the involvement of HSPGs, and manipulations of this enzyme do not reduce the synthesis of other proteoglycan subtypes (14, 26, 28, 49). *Ext1* knockdown inhibited the internalization of tau aggregates into primary hippocampal neurons without affecting clathrin-mediated uptake of transferrin. Thus, pharmacologic and genetic interventions demonstrate that HSPGs are critical mediators of tau fibril internalization. Tau binding to HSPGs was also required for transcellular propagation in cell culture, as introduction to the media of heparin or the heparin mimetic F6 prevented recombinant and cell-derived tau fibrils from nucleating further aggregation. Finally, we confirmed the involvement of tau/HSPG binding in vivo by stereotactic injection of tau fibrils into the cortex of WT mice. F6 blocked aggregate uptake into neurons without affecting transferrin uptake. Taken together, this work suggests that recombinant tau fibrils and tau aggregates produced within a cell use HSPG binding to seed further aggregation within recipient cells.

Tau and α-Synuclein Use Similar Modes of Cell Uptake. Our data suggest strongly that tau and α-synuclein fibrils use the same

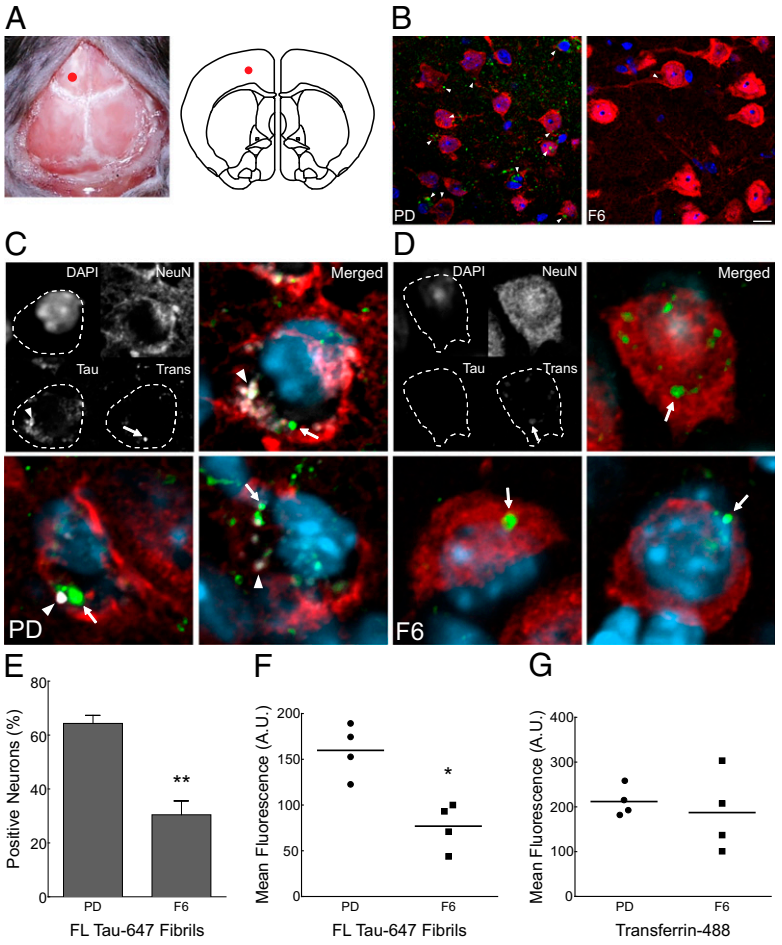

Fig. 7. HSPGs mediate internalization of FL tau fibrils in vivo. (*A*) Schematic representation of stereotactic injection site. (*B*) Injection of FL tau fibrils with heparin mimetic F6 leads to a reduction of fibril internalization by cortical neurons. Mice (n = 3 per group) were injected with 472 ng of FL tau-488 fibrils (green) and 1 μg of PD or F6. Brain sections were immunostained with anti-NeuN antibody to label neurons (red) and counterstained with DAPI (blue). Arrowheads designate FL tau fibrils associated with neurons. (Scale bar: 10 μm.) (*C* and *D*) Heparin mimetic F6 blocks FL tau fibril uptake, but not Tfn-488. Mice (n = 4 per group) were injected with 472 ng of FL tau-647 fibrils (white), 5 μg of Tfn-488 (green), and 1 μg of PD or F6. Injection of tau fibrils and transferrin with PD resulted in entry of both proteins into neurons, whereas coinjection with F6 resulted in the selective inhibition of tau fibril entry. The grayscale images are single channel fluorescence images corresponding to the multichannel images labeled as "merged." Arrowheads designate FL tau fibrils; long arrows designate transferrin. (*E*) Quantification of tau-positive neurons from experiment *C* and *D*. A total of 494 and 660 neurons were counted and averaged in the PD and F6 conditions, respectively, from four male mice per cohort. Error bars show SEM (**$P < 0.01$, Student t test). (*F* and *G*) Quantification of neuronal fluorescence intensity from experiment *C* and *D*. Mean fluorescence intensity of tau fibrils and transferrin were calculated per neuron and averaged from individual mice, each represented by a single data point ($P = 0.028$, Mann–Whitney U test, two-tailed exact significance) comparing treatment effects on tau fibril uptake.

mechanism of uptake into cells. Fibrils of these proteins each colocalize with HSPGs, TAT peptide, and with each other when analyzed by confocal microscopy. Further, both are equivalently sensitive to heparin and chlorate inhibition. These mechanisms of uptake are specific, because Htt(Q50) fibrils failed to colocalize with tau, α-synuclein, or TAT, and were not sensitive to heparin or chlorate. Htt(Q50) fibrils nonetheless seeded aggregation of intracellular Htt(Q25)CFP/YFP, indicating that at least two modes exist for propagation of seeding activity from the outside to the inside of the cell. The primary route of Htt internalization remains unclear, although undefined cell surface proteins have been implicated (34). Unlike tau and α-synuclein, Htt exon 1 does not feature a clear heparin-binding domain. Indeed, at least one study has suggested that Htt fibrils directly penetrate the cell membrane to enter the cytosol before being sequestered in aggresomes (35). These distinct uptake mechanisms have obvious implications for further studies and for consideration of therapeutic targets.

Tau/HSPG Binding as a Therapeutic Target. It has been known for almost two decades that tau is a heparin-binding protein (25), and thus could theoretically bind HSPGs. Because tau is cytosolic, however, it was not clear if this interaction held physiological significance. With the knowledge that tau is present in the extracellular space (12, 47, 50), we hypothesized that the tau/HSPG interaction plays a key role in transcellular propagation of pathologic processes. In the presence of compounds predicted to block tau fibril binding to HSPGs, tau failed to bind the cell surface, enter cells, or seed further intracellular aggregation. α-Synuclein aggregates also colocalized with HSPGs, and their uptake and seeding was similarly heparin-sensitive. In addition to α-synuclein, we speculate that other proteins associated with spreading pathology, such as SOD1, could also use this pathway. SOD3, the extracellular paralogue of SOD1, is a known ligand of HSPGs, and it is possible that SOD1 may also contain heparin-binding domains (27). In our study, heparin did not block internalization and seeding of Htt(Q50) fibrils, suggesting an alternate internalization pathway for this protein. Tau,

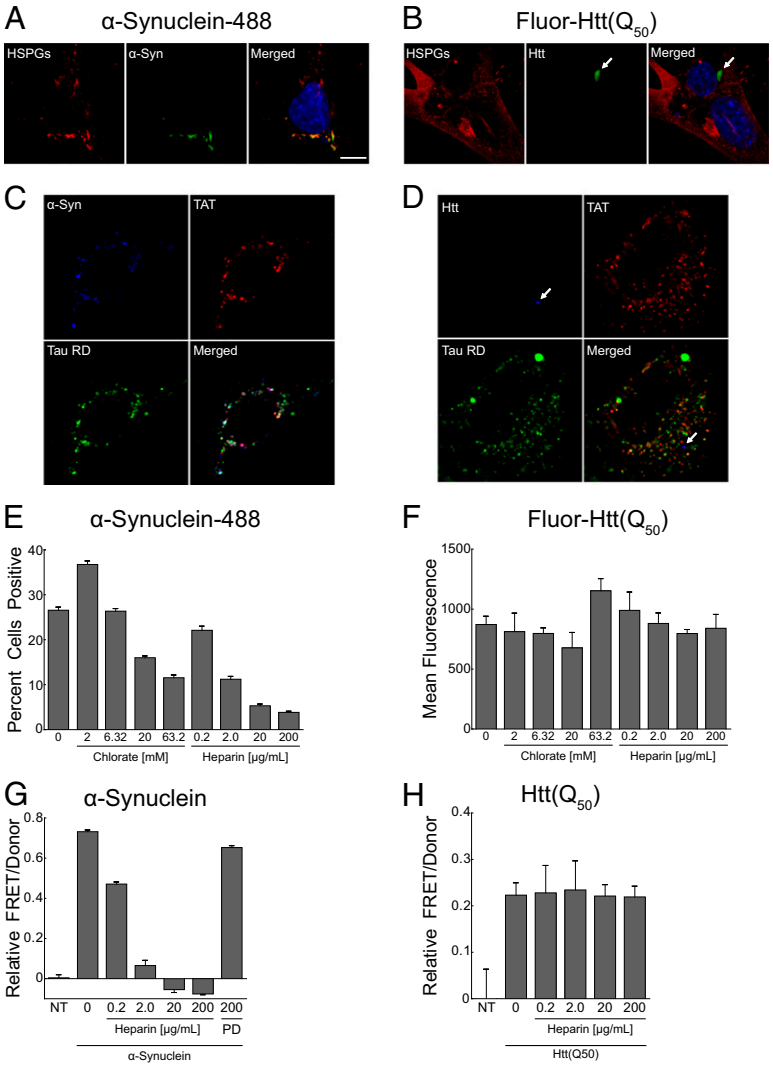

Fig. 8. HSPGs mediate internalization and seeding of α-synuclein but not huntingtin fibrils. (*A* and *B*) Uptake of α-synuclein-488 and fluorescein-Htt exon1(Q50) fibrils (green) into C17.2 cells counterstained with anti-HSPG antibody (red) and DAPI (blue). (*A*) α-Synuclein-488 (200 nM) colocalizes with HSPGs. (*B*) Htt(Q50) fibrils (5 μM) do not colocalize with HSPGs. (Scale bar: 10 μM.) (*C* and *D*) α-Synuclein fibrils (blue) colocalize with TAT (red) and tau (green), whereas Htt(Q50) fibrils (blue) do not. (*E* and *F*) Heparin and chlorate dose dependently decrease the internalization of α-synuclein, but not Htt(Q50) fibrils, into C17.2 cells, as measured by automated microscopy analysis. α-Synuclein fibrils (100 nM) and Htt(Q50) fibrils (1 μM) were applied to cells for 5 h before harvesting for microscopy or flow cytometry. Approximately 40,000 cells were analyzed for each α-synuclein condition; ∼12,000 cells were analyzed for each Htt(Q50) condition, and all were run in triplicate. (*G* and *H*) Heparin blocks seeding by α-synuclein fibrils, but not Htt(Q50) fibrils. HEK293 cells cotransfected with α-synuclein-CFP/YFP or Htt exon1(Q25)-CFP/YFP were cotreated with unlabeled α-synuclein fibrils (100 nM) or Htt exon1(Q50) fibrils (1 μM), along with heparin or PD for 24 h before reading FRET measurements. FRET values reflect subtraction of signal from the nontreated (NT) group.

α-synuclein, and SOD1 share many biophysical properties, and it is highly plausible that they exploit similar cellular pathways to propagate misfolding between cells. Thus, pharmacologic interventions designed to block HSPG binding could be broadly applicable, whether by targeting binding motifs within fibrils or modifying the HSPGs themselves. Indeed, heparin mimetics have demonstrated efficacy in the inhibition of prion pathogenesis in animal models (51). Although tau/HSPG interactions are not yet a proven therapeutic target, our hypothesis makes straightforward and testable predictions for preclinical studies and for future drug design and discovery.

Materials and Methods

Tau Expression, Purification, Fibrillization, and Labeling. FL tau (2N4R isoform) and the tau RD, composed of amino acids 243 to 375, with an HA tag (YPYDVPDYA) on their C termini, were subcloned into pRK172. Recombinant FL tau and tau RD were prepared as described previously (52) from Rosetta (DE3) pLacI competent cells (Novagen). To induce fibrillization of tau monomer, 8μM tau RD was preincubated at room temperature in 10 mM DTT for 60 min followed by incubation at 37 °C in 10 mM Hepes, 100 mM NaCl, and 8 μM heparin for 24 h without agitation; FL tau monomer was incubated for 48 h to form fibrils. For experiments requiring fluorescent detection of tau, 200 μL of 8 μM tau protein or buffer was incubated with 0.025mg of Alexa Fluor succinimidyl ester dyes overnight at 4 °C. Excess dye was quenched with 100 mM glycine for 1 h. Immediately before use, fibrils were sonicated using the Sonicator 3000 (Misonex) at a power of 3 for 30 s.

Immunofluorescence and Microscopy. All cells were grown on μ-Slides (Ibidi) for imaging by microscopy. For propidium iodide staining, cells were coincubated with tau RD-488 fibrils, tau monomer, tau buffer, or 5% (vol/vol) ethanol and propidium iodide (5 μg/mL; Sigma) for 3 h, washed twice with PBS solution, and examined by confocal microscopy. For clathrin heavy chain (CHC) and caveolin-1 immunofluorescence, cells were treated with 150 nM tau RD-488 fibrils for 1 h, extensively washed with PBS solution, and fixed with 4% PFA. Cells were stained with α-CHC mouse monoclonal antibody (1:300; Covance) or caveolin-1 mouse monoclonal antibody (1:500; Santa

Cruz), followed by secondary labeling with Alexa Fluor-546 goat anti-mouse (1:1,000; Molecular Probes) and DAPI. For phalloidin staining, cells were incubated with 150 nM tau RD-488 or Alexa Fluor 488-containing buffer for the time indicated, washed, fixed as described earlier, and stained with 33nM rhodamine-phalloidin (Invitrogen) for 20 min. For colocalization studies between tau RD and the TAT peptide, 150 nM of tau RD-488 fibrils and 5 μM TAT-TAMRA peptide (residues 47–57; AnaSpec) were coadministered to C17.2 cells for 90 min. Cells were then extensively washed with media. To quench extracellular fluorescence, trypan blue (0.05% in PBS solution; Sigma) was added to the cells for 15 s and removed. Cells were washed twice and immediately imaged live in phenol red-free DMEM (1% FBS) by using confocal microscopy with an environmental chamber (5% CO_2 at 37 °C). For colocalization studies between tau RD and HSPGs, 150 nM of tau RD-488 fibrils were administered to C17.2 cells for 90 min. Cells were trypsinized for 5 min, followed by replating on Ibidi μ-Slides. Cells were allowed to recover for 3.5 h before fixation in 4% PFA. HSPGs were immunostained with anti-10E4 antibody (1:100; US Biological), followed by secondary labeling with Alexa Fluor-546 goat anti-mouse (1:1,000; Molecular Probes), and images were captured by using confocal microscopy.

For immunohistochemistry of mouse brain sections, sections were immunostained with α-NeuN antibody (1:200; Millipore) followed by secondary labeling with Alexa Fluor-546 goat anti-mouse and DAPI. Images for quantification were collected such that only brain regions 150 to 300 μM away (medial/lateral) from the injection sites were included. This was done to avoid regions saturated or void of injected material. In the dorsal/ventral axis, images were collected along the entire length of the injection tract. Images were acquired from five sections per animal including the midpoint of the injection site, ±25 μM and ±50 μM (rostral/caudal) from the injection site. Quantification of images was conducted by using ImageJ (National Institutes of Health). For quantification of percent neurons positive for tau aggregates, regions of interest (ROIs) were drawn around cells based on NeuN staining. The fluorescence signal threshold was applied equally to all sections, and cells were counted as positive if a fluorescence puncta fell within the boundary of the ROI. For quantification of mean fluorescent intensity, cells were measured by using the same ROIs as described earlier without fluorescence signal threshold. All cells were counted that had a discernible DAPI and NeuN stain.

The 3D projection was created by acquiring a series of confocal images of a neuron at an interval of 0.2 μM sections over a span of 3 μM. VolViewer software was used to create a ray sum projection from individual images, and Adobe After Effects was used to animate the projection.

Flow Cytometry. C17.2 cells were plated at 25,000 cells per well in a 24-well plate. The next day, cells were pretreated with the following drugs for 30 min: cytochalasin D (1 μM; Sigma), latrunculin A (3 μM; Invitrogen), amiloride hydrochloride hydrate (1 mM; Sigma), rottlerin (30 μM; Sigma), and Dynasore (80 μM; Sigma). Cells were next treated with tau RD-488 fibrils or Alexa Fluor-488–containing buffer for 3 h. Cells were harvested with 0.25% trypsin for 5 min and resuspended in HBSS plus 1% FBS and 1 mM EDTA before flow cytometry. Cells were counted in a FACScan flow cytometer (BD Biosciences) or MACSQuant VYB (Miltenyi Biotec). Each experiment was conducted three times, and 25,000 cells were counted in each individual experiment. For tau fibril-binding experiments, cells or tau fibrils were pretreated separately with the indicated concentrations of sodium chlorate or heparin (Sigma), respectively, for 12 h. Cells were then equilibrated for 4 °C for 15 min before the addition of tau fibrils for 60 min at 4 °C, suspended in cell dissociation solution (Sigma), and subjected to flow cytometry.

Automated Microscopy Analysis. After RD-488 fibril or dextran fluorescein (70 kD, anionic, lysine fixable) treatment, cells were trypsinized for 5 min, replated on a 96-well plate, allowed to recover for 3.5 h, and fixed. To identify cell boundaries, cells were stained with 10 μg/mL of wheat germ agglutinin labeled with Alexa Fluor-647 followed by DNA staining with DAPI. Cells and intracellular puncta were visualized by automated microscopy by using an InCell Analyzer 1000 high-content microscope fitted with a 10× objective (GE Healthcare). ROIs were defined by user-assigned size and fluorescence intensity thresholds and were quantified with the Multi-Target Analysis Module of the IN Cell Analyzer 1000 Workstation 3.7 analysis software. For tau fibril internalization experiments, cells were pretreated with chlorate for 12 h or heparinase III or chondroitinase AC (Ibex) for 3 h before fibril treatment. Similarly, tau fibrils were pretreated with heparin for 12 h before addition of the heparin–fibril complexes.

Cell Culture and Transfections. HEK293 cells were cultured in DMEM supplemented with 10% FBS, 100 μg/mL penicillin, and 100 μg/mL streptomycin. Cultures were maintained in a humidified atmosphere of 5% CO_2 at 37 °C. For transient transfections, cells plated in complete medium were transfected by using Lipofectamine 2000 (Invitrogen) and 600 ng of appropriate DNA constructs according to the manufacturer's recommendations and harvested 24 h later for further analyses. To culture primary neurons, the cortex or hippocampus of embryonic day 18.5 mouse embryos was isolated and digested with 2 mg/mL papain and 0.1% DNase I. Neurons in Neurobasal media containing serum-free B-27 and GlutaMAX were then seeded on culture plates precoated with 10 μg/mL poly-D-lysine and 1.5 μg/cm^2 laminin. Medium was changed once every 4 d until neurons were ready for use.

FRET Assays. Total tau aggregation was measured by an assay based on FRET between RD(ΔK)-CFP/YFP, which has been described previously (12). The FRET calculations provide a reproducible measure of intracellular aggregation, and take into account the relative amounts of donor and acceptor proteins (53–55). For seeded aggregation experiments, HEK293 cells were transfected with 150 ng of tau RD(ΔK)-CFP and 450 ng of tau RD(ΔK)-YFP. Twenty-four hours later, cells were split into a 96-well plate and allowed to recover overnight. Tau RD fibrils (50 nM) were preincubated with heparin or F6 at the indicated concentrations for 12 h and then applied to cells for 24 h to induce intracellular aggregation. Heparinase III was applied directly to the cell media for 3 h before the application of tau RD fibrils for 24 h. For transcellular propagation experiments, acceptor cells were transfected as described earlier; donor cells were transfected with 600 ng of tau RD(LM)-HA. After 24 h, cells were split into 96-well plates at equal percentages of donor and acceptor populations and cocultured for 48 h in the presence or absence of heparin, F6, or heparinase III. Spectral FRET measurements (FRET/donor) were obtained by using a Tecan M1000 fluorescence plate reader according to methods described previously (12, 53). Excitation and emission optima were as follows: CFP, 435 nm excitation/485 nm emission; YFP, 485 nm excitation/527 nm emission; and FRET, 435 nm excitation/527 nm emission.

Stereotactic Injections. Male C57BL6/J mice (5 mo of age) were injected by using a 30-gauge Hamilton microsyringe in the left cortex (anteroposterior, +1.3 mm; mediolateral, +1.5 mm; dorsoventral, −1.6 mm relative to bregma) at an infusion rate of 0.1 μL/min. For qualitative microscopy studies, 472 ng of FL Tau-488 fibrils were coinjected with 1 μg of F6 or PD (final volume 1.1 μL; n = 3 animals per group). For quantitative microscopy studies, 472 ng of FL Tau-647 fibrils plus 5 μg of Tfn-488 were coinjected with 1 μg of F6 or PD (final volume, 2.1 μL; n = 4 animals per group). Animals were killed 48 h after injection with 0.03% heparin in chilled PBS solution, and brains were postfixed in 4% PFA for 24 h. For tissue processing, brains were sectioned at 25 μM on a cryostat and preserved in cryoprotectant with 30% sucrose.

ACKNOWLEDGMENTS. We thank Josiah Gerdts for help with Movie S1 and the Alvin J. Siteman Cancer Center at Washington University School of Medicine and Barnes–Jewish Hospital for the use of the Siteman Flow Cytometry Core, which provided flow cytometry service. This work was supported by the Tau Consortium; the Muscular Dystrophy Association; the American Health Assistance Foundation; the Ruth K. Broad Foundation; National Institutes of Health (NIH) Grants 1R01NS071835 (to M.I.D.), 1R01GM038093 (to F.M.B.), K08NS074194 (to T.M.M.), 1F31NS079039 (to B.B.H.), P50 CA94056 (Molecular Imaging Center, Mallinckrodt Institute of Radiology, Washington University School of Medicine), and P30 CA091842 (National Cancer Institute Cancer Center Support Grant to Siteman Cancer Center, Washington University School of Medicine); the Molecular Imaging Center at the Mallinckrodt Institute of Radiology; the Bridging Research with Imaging, Genomics, and High-Throughput Technologies Institute at Washington University School of Medicine; and an Anheuser-Busch/Emerson challenge gift. The Hope Center Alafi Neuroimaging Laboratory and the Bakewell Neuroimaging Core are supported in part by the Bakewell Family Foundation and NIH Neuroscience Blueprint Interdisciplinary Center Core Grant P30 NS057105 (to Washington University).

1. Seeley WW, Crawford RK, Zhou J, Miller BL, Greicius MD (2009) Neurodegenerative diseases target large-scale human brain networks. *Neuron* 62(1):42–52.
2. Zhou J, Gennatas ED, Kramer JH, Miller BL, Seeley WW (2012) Predicting regional neurodegeneration from the healthy brain functional connectome. *Neuron* 73(6):1216–1227.
3. Braak H, Braak E (1997) Diagnostic criteria for neuropathologic assessment of Alzheimer's disease. *Neurobiol Aging* 18(4, suppl):S85–S88.
4. Raj A, Kuceyeski A, Weiner M (2012) A network diffusion model of disease progression in dementia. *Neuron* 73(6):1204–1215.

5. Braak H, Braak E (1991) Neuropathological stageing of Alzheimer-related changes. *Acta Neuropathol* 82(4):239–259.
6. Frost B, Jacks RL, Diamond MI (2009) Propagation of tau misfolding from the outside to the inside of a cell. *J Biol Chem* 284(19):12845–12852.
7. Clavaguera F, et al. (2009) Transmission and spreading of tauopathy in transgenic mouse brain. *Nat Cell Biol* 11(7):909–913.
8. Liu L, et al. (2012) Trans-synaptic spread of tau pathology in vivo. *PLoS ONE* 7(2): e31302.
9. de Calignon A, et al. (2012) Propagation of tau pathology in a model of early Alzheimer's disease. *Neuron* 73(4):685–697.
10. Guo JL, Lee VMY (2011) Seeding of normal Tau by pathological Tau conformers drives pathogenesis of Alzheimer-like tangles. *J Biol Chem* 286(17):15317–15331.
11. Iba M, et al. (2013) Synthetic tau fibrils mediate transmission of neurofibrillary tangles in a transgenic mouse model of Alzheimer's-like tauopathy. *J Neurosci* 33(3):1024–1037.
12. Kfoury N, Holmes BB, Jiang H, Holtzman DM, Diamond MI (2012) Trans-cellular propagation of Tau aggregation by fibrillar species. *J Biol Chem* 287(23): 19440–19451.
13. Schonberger O, et al. (2003) Novel heparan mimetics potently inhibit the scrapie prion protein and its endocytosis. *Biochem Biophys Res Commun* 312(2):473–479.
14. Horonchik L, et al. (2005) Heparan sulfate is a cellular receptor for purified infectious prions. *J Biol Chem* 280(17):17062–17067.
15. Mercer J, Helenius A (2009) Virus entry by macropinocytosis. *Nat Cell Biol* 11(5): 510–520.
16. Kaplan IM, Wadia JS, Dowdy SF (2005) Cationic TAT peptide transduction domain enters cells by macropinocytosis. *J Control Release* 102(1):247–253.
17. Wadia JS, Stan RV, Dowdy SF (2004) Transducible TAT-HA fusogenic peptide enhances escape of TAT-fusion proteins after lipid raft macropinocytosis. *Nat Med* 10(3): 310–315.
18. Nakase I, et al. (2004) Cellular uptake of arginine-rich peptides: roles for macropinocytosis and actin rearrangement. *Mol Ther* 10(6):1011–1022.
19. Nakase I, et al. (2007) Interaction of arginine-rich peptides with membrane-associated proteoglycans is crucial for induction of actin organization and macropinocytosis. *Biochemistry* 46(2):492–501.
20. Chang HC, Samaniego F, Nair BC, Buonaguro L, Ensoli B (1997) HIV-1 Tat protein exits from cells via a leaderless secretory pathway and binds to extracellular matrix-associated heparan sulfate proteoglycans through its basic region. *AIDS* 11(12): 1421–1431.
21. Tyagi M, Rusnati M, Presta M, Giacca M (2001) Internalization of HIV-1 tat requires cell surface heparan sulfate proteoglycans. *J Biol Chem* 276(5):3254–3261.
22. Rusnati M, et al. (1997) Interaction of HIV-1 Tat protein with heparin. Role of the backbone structure, sulfation, and size. *J Biol Chem* 272(17):11313–11320.
23. Liu Y, et al. (2000) Uptake of HIV-1 tat protein mediated by low-density lipoprotein receptor-related protein disrupts the neuronal metabolic balance of the receptor ligands. *Nat Med* 6(12):1380–1387.
24. Console S, Marty C, García-Echeverría C, Schwendener R, Ballmer-Hofer K (2003) Antennapedia and HIV transactivator of transcription (TAT) "protein transduction domains" promote endocytosis of high molecular weight cargo upon binding to cell surface glycosaminoglycans. *J Biol Chem* 278(37):35109–35114.
25. Goedert M, et al. (1996) Assembly of microtubule-associated protein tau into Alzheimer-like filaments induced by sulphated glycosaminoglycans. *Nature* 383(6600): 550–553.
26. Kanekiyo T, et al. (2011) Heparan sulphate proteoglycan and the low-density lipoprotein receptor-related protein 1 constitute major pathways for neuronal amyloid-beta uptake. *J Neurosci* 31(5):1644–1651.
27. Conrad EH (1998) *Heparin-Binding Proteins* (Academic, San Diego).
28. Lidholt K, et al. (1992) A single mutation affects both N-acetylglucosaminyltransferase and glucuronosyltransferase activities in a Chinese hamster ovary cell mutant defective in heparan sulfate biosynthesis. *Proc Natl Acad Sci USA* 89(6):2267–2271.
29. Tong M, et al. (2008) RGTA OTR 4120, a heparan sulfate proteoglycan mimetic, increases wound breaking strength and vasodilatory capability in healing rat full-thickness excisional wounds. *Wound Repair Regen* 16(2):294–299.
30. Ouidja MO, et al. (2007) Structure-activity studies of heparan mimetic polyanions for anti-prion therapies. *Biochem Biophys Res Commun* 363(1):95–100.
31. Desplats P, et al. (2009) Inclusion formation and neuronal cell death through neuron-to-neuron transmission of alpha-synuclein. *Proc Natl Acad Sci USA* 106(31): 13010–13015.
32. Hansen C, et al. (2011) α-Synuclein propagates from mouse brain to grafted dopaminergic neurons and seeds aggregation in cultured human cells. *J Clin Invest* 121(2):715–725.
33. Luk KC, et al. (2009) Exogenous alpha-synuclein fibrils seed the formation of Lewy body-like intracellular inclusions in cultured cells. *Proc Natl Acad Sci USA* 106(47): 20051–20056.
34. Trevino RS, et al. (2012) Fibrillar structure and charge determine the interaction of polyglutamine protein aggregates with the cell surface. *J Biol Chem* 287(35): 29722–29728.
35. Ren PH, et al. (2009) Cytoplasmic penetration and persistent infection of mammalian cells by polyglutamine aggregates. *Nat Cell Biol* 11(2):219–225.
36. Münch C, O'Brien J, Bertolotti A (2011) Prion-like propagation of mutant superoxide dismutase-1 misfolding in neuronal cells. *Proc Natl Acad Sci USA* 108(9):3548–3553.
37. Wadia JS, Schaller M, Williamson RA, Dowdy SF (2008) Pathologic prion protein infects cells by lipid-raft dependent macropinocytosis. *PLoS ONE* 3(10):e3314.
38. Lee HJ, et al. (2008) Assembly-dependent endocytosis and clearance of extracellular alpha-synuclein. *Int J Biochem Cell Biol* 40(9):1835–1849.
39. de Planque MR, et al. (2007) beta-Sheet structured beta-amyloid(1-40) perturbs phosphatidylcholine model membranes. *J Mol Biol* 368(4):982–997.
40. Blumenthal R, Seth P, Willingham MC, Pastan I (1986) pH-dependent lysis of liposomes by adenovirus. *Biochemistry* 25(8):2231–2237.
41. Chandran K, Farsetta DL, Nibert ML (2002) Strategy for nonenveloped virus entry: A hydrophobic conformer of the reovirus membrane penetration protein micro 1 mediates membrane disruption. *J Virol* 76(19):9920–9933.
42. Conner SD, Schmid SL (2003) Regulated portals of entry into the cell. *Nature* 422(6927):37–44.
43. Flach K, et al. (2012) Tau oligomers impair artificial membrane integrity and cellular viability. *J Biol Chem* 287(52):43223–43233.
44. Vieira TCRG, et al. (2011) Heparin binding by murine recombinant prion protein leads to transient aggregation and formation of RNA-resistant species. *J Am Chem Soc* 133(2):334–344.
45. Watson DJ, Lander AD, Selkoe DJ (1997) Heparin-binding properties of the amyloidogenic peptides Abeta and amylin. Dependence on aggregation state and inhibition by Congo red. *J Biol Chem* 272(50):31617–31624.
46. Cohlberg JA, Li J, Uversky VN, Fink AL (2002) Heparin and other glycosaminoglycans stimulate the formation of amyloid fibrils from alpha-synuclein in vitro. *Biochemistry* 41(5):1502–1511.
47. Yamada K, et al. (2011) In vivo microdialysis reveals age-dependent decrease of brain interstitial fluid tau levels in P301S human tau transgenic mice. *J Neurosci* 31(37): 13110–13117.
48. Okada M, Nadanaka S, Shoji N, Tamura J, Kitagawa H (2010) Biosynthesis of heparan sulfate in EXT1-deficient cells. *Biochem J* 428(3):463–471.
49. Broekelmann TJ, et al. (2005) Tropoelastin interacts with cell-surface glycosaminoglycans via its COOH-terminal domain. *J Biol Chem* 280(49):40939–40947.
50. Lee S, Kim W, Li Z, Hall GF (2012) Accumulation of vesicle-associated human tau in distal dendrites drives degeneration and tau secretion in an in situ cellular tauopathy model. *Int J Alzheimers Dis* 2012:172837.
51. Doh-ura K, et al. (2004) Treatment of transmissible spongiform encephalopathy by intraventricular drug infusion in animal models. *J Virol* 78(10):4999–5006.
52. Goedert M, Jakes R (1990) Expression of separate isoforms of human tau protein: correlation with the tau pattern in brain and effects on tubulin polymerization. *EMBO J* 9(13):4225–4230.
53. Pollitt SK, et al. (2003) A rapid cellular FRET assay of polyglutamine aggregation identifies a novel inhibitor. *Neuron* 40(4):685–694.
54. Desai UA, et al. (2006) Biologically active molecules that reduce polyglutamine aggregation and toxicity. *Hum Mol Genet* 15(13):2114–2124.
55. Shao J, Welch WJ, Diamond MI (2008) ROCK and PRK-2 mediate the inhibitory effect of Y-27632 on polyglutamine aggregation. *FEBS Lett* 582(12):1637–1642.

Supporting Information

Holmes et al. 10.1073/pnas.1301440110

SI Text

Tau Fibril Entry Is an Active Process. Many studies have proposed that amyloid fibrils can directly permeabilize membranes, producing cellular toxicity and potentially providing a direct route to cell entry. We tested this possibility for tau fibrils with cultured cells. We administered tau repeat domain (RD) fibrils or monomer tagged with Alexa Fluor-488 dye to the medium of C17.2 cells, in conjunction with propidium iodide (PI) to indicate membrane disruption. Monomer equivalent of tau fibrils (150 nM) did not increase PI positivity, whereas 5% ethanol caused 72% of cells to score positive. Thus, we found no evidence for direct membrane permeabilization (Fig. S1 *A* and *B*). We tested for saturable uptake by incubating cells with increasing molar concentrations of RD fibrils for 30 min, harvesting the cells by trypsinization (to remove all extracellular tau), followed by Western blot for tau. Maximal RD fibril internalization occurred between 0.67 and 1.33 μM (Fig. S1 *C* and *D*), consistent with a saturable transport mechanism. We next tested for temperature dependence of tau uptake by comparing cells exposed at 37 °C vs. 4 °C. At 4 °C, a nonpermissive temperature for endocytosis, RD fibril uptake was virtually abolished (Fig. S1*E*). Additionally, ATP depletion by sodium azide and deoxyglucose decreased tau fibril uptake as measured by Western blot (Fig. S1*F*). Our data indicate that an active process of endocytosis is most likely.

Tau Fibril Uptake Is Independent of Clathrin or Caveolin. We excluded a role for clathrin- and caveolin-mediated endocytosis in tau fibril uptake. We first blocked clathrin-mediated endocytosis by siRNA knockdown of clathrin heavy chain (CHC) in cultured cells (Fig. S2*A*). CHC knockdown was confirmed by Western blot to monitor CHC protein levels (Fig. S2*B*). We observed robust tau aggregate uptake, even in the presence of significant CHC knockdown. This response was quantified by counting cells (Fig. S2 *C* and *D*). We next tested for colocalization of internalized tau aggregates with caveolin by staining cells with anti-caveolin antibody. We did not find any appreciable colocalization between tau and caveolin (Fig. S2*E*).

SI Materials and Methods

EM. To image tau RD fibrils directly, 5 μL of 4 μM tau RD fibril suspension was placed on a 3 × 3 mm chromo-sulfuric acid-cleaned, water-washed, and air-dried glass coverslip chip and allowed to rest for 5 min. The sample was rinsed once with distilled H_2O and immediately quick-frozen. To image tau fibrils associated with cells, C17.2 cells treated with 150 nM of tau RD fibrils were cultured on 3 × 3-mm glass coverslips, washed for 5 min in mammalian Ringer solution at 37 °C, and transferred to a dish of 2% glutaraldehyde in 100 mM NaCl, 30 mM Hepes, 2 mM $CaCl_2$, pH 7.2 (NaHCa), for 1 h at room temperature. Just before freezing, glass chips were rinsed in three exchanges of distilled H_2O and quick-frozen. Quick-freeze deep-etch EM was performed according to published protocol, with minor modifications (1). Before freezing, glass slips were rinsed with distilled H_2O and frozen by forceful impact against a pure copper block cooled to 4 K with liquid helium. Frozen samples were mounted in a Balzers 400 vacuum evaporator, etched for 20 min at −80 °C, and rotary-replicated with ∼3 nm platinum deposited from a 15° angle above the horizontal, followed by ∼10 nm stabilization film of pure carbon deposited from a 45° angle. Replicas were floated onto a dish of concentrated hydrofluoric acid and transferred through several rinses of distilled H_2O, all containing a loopful of Photo-Flo, picked up on Formvar-coated copper grids, and photographed with a JEOL 100CX transmission electron microscope with an attached AMT digital camera.

Surface Plasmon Resonance. Surface plasmon resonance (SPR) experiments were performs on BIAcore 2000 SPR instrument (GE Healthcare-BIAcore). BIAcore sensor chip CM-5 (GE Healthcare) was activated by using 1-ethyl-3-(3-dimethylaminopropyl)-carbodiimide and NHS in 1:1 ratio for 7 min. One flow cell was immobilized with RD tau fibrils (20 μg/mL in 10 mM sodium acetate, pH 4.0) on a Biacore CM-5 sensor chip at a flow rate of 5 μL/min. The remaining unbound area was deactivated by passage of 1 M ethanolamine, pH 8.5. One flow cell was used as a reference cell by activating and blocking with 1 M ethanolamine without any protein. Then, TAT peptide and HJ9.3 antibody were injected at the indicated concentrations in filtered, degassed 0.01 M Hepes buffer, 0.15 M NaCl, 0.005% surfactant P20, pH 7.4, at a flow rate of 10 μL/min. All the samples were run in duplicate. After each run with a single peptide or antibody concentration, the surface of the chip was regenerated by using 10 mM glycine, pH 1.7, to remove the bound RD tau fibrils. Data analysis was performed by using BIAevaluation software (GE Healthcare-BIAcore).

Lentiviral Transduction and Quantitative RT-PCR. *Ext1* shRNA viral vectors from the RNAi Consortium collection (1) were acquired from the Washington University RNAi Core (target sequence, CCCTTACTACTATGCTAATTT). *Ext1* and *luciferase* shRNA control viral vectors were used to produce lentiviral particles as described previously (2). Lentivirus containing media was concentrated 10× by using a LentiX Concentrator (Clontech), and 2 μL of virus suspension was added to mouse primary hippocampal neurons at 0 d in vitro (DIV) in a final volume of 200 μL. Neurons were treated with FL tau-488 fibrils or transferrin-488 on DIV 7 for 3 h before analysis by flow cytometry. Knockdown efficiency of *Ext1* shRNA was tested by using C17.2 neuronal cell lines grown in 24-well plates. A total of 5 μL of *Ext1* virus suspension was added in a final volume of 500 μL of complete media. RNA was harvested 7 d after transduction and purified by using the RNeasy kit (Qiagen). Transcript levels relative to GAPDH were determined by quantitative PCR (ΔCT method) by using an ABI Prism 7900HT sequence detection instrument (Applied Biosystems).

Preparation of α-Synuclein and Huntingtin Fibrils. Recombinant α-synuclein protein was produced in *Escherichia coli* by using previously described methods (3, 4). α-Synuclein protein was dialyzed overnight in 10 mM Tris-HCl, pH 7.6, 50 mM NaCl, 1 mM DTT. Recombinant α-synuclein monomer (2 mg/mL) was incubated in 20 mM Tris-HCl, pH 8.0, 100 mM NaCl for 72 h at 37 °C with shaking at 1,000 rpm in an Eppendorf Thermomixer R (Eppendorf North America, Hauppauge, NY; cat. 022670107) to induce fibrillization. Fibril concentration was calculated by centrifuging the fibril reaction mix at 15,000 × *g* for 15 min to separate fibrils from monomer. The concentration of α-synuclein monomer in the supernatant was determined in a BCA protein assay according to the manufacturer's instructions, using a BSA standard curve. The measured decrease in α-synuclein monomer concentration was used to determine the concentration of fibrils in the 72 h fibril reaction mixture.

Synthetic Htt(Q50), comprising the exon 1 fragment, was synthesized with fluorescein conjugated via the N-terminal primary amine by Fmoc chemistry at the Keck Biotechnology Resource Laboratory of Yale University. Crude peptide was solubilized in

formic acid and dialyzed into phosphate buffer solution. Fibrillization of Htt(Q50) occurred at room temperature for 24 h.

All aggregates were sonicated by using a Sonicator 3000 (Misonex) at a power of 3 for 30 s immediately before use.

1. Moffat J, et al. (2006) A lentiviral RNAi library for human and mouse genes applied to an arrayed viral high-content screen. *Cell* 124(6):1283–1298.
2. Sasaki Y, Vohra BP, Baloh RH, Milbrandt J (2009) Transgenic mice expressing the Nmnat1 protein manifest robust delay in axonal degeneration in vivo. *J Neurosci* 29 (20):6526–6534.
3. Giasson BI, et al. (2003) Initiation and synergistic fibrillization of tau and alpha-synuclein. *Science* 300(5619):636–640.
4. Huang C, Ren G, Zhou H, Wang CC (2005) A new method for purification of recombinant human alpha-synuclein in Escherichia coli. *Protein Expr Purif* 42(1): 173–177.

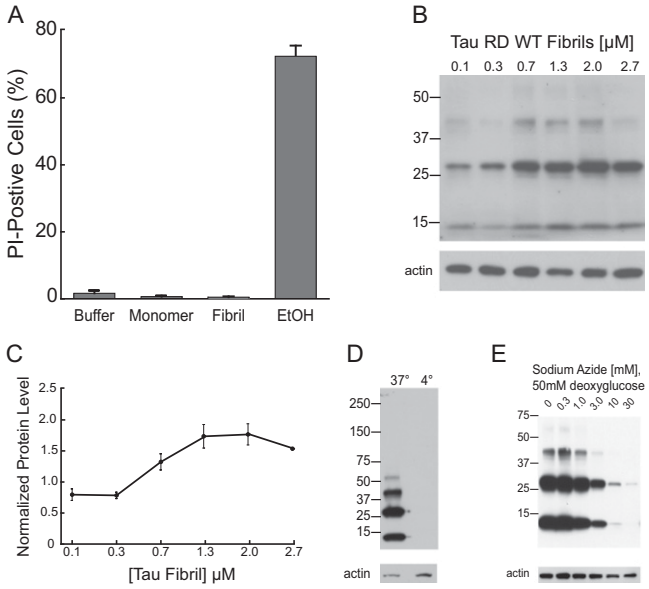

Fig. S1. Recombinant tau RD fibrils are actively internalized by C17.2 neural cells in culture. (*A*) Tau RD fibrils do not disrupt the plasma membrane. Cells were incubated with 150 nM Tau RD-488 fibrils, monomer, buffer, and PI for 3 h. Cells were incubated for the same period with 5% ethanol as a positive control for PI staining. The percentage of PI-positive cells was quantified by direct counting via microscopy ($n = 4$ replicates per experiment, 100 cells counted per replicate). (*B*) Tau RD fibril internalization is saturable. Cells were incubated with tau RD-HA fibrils at the indicated concentrations for 30 min. Trypsinized cell lysates were loaded onto a gradient gel and tau RD fibrils were probed with an anti-HA antibody. (*C*) Quantification of data from *B* from two separate Western blots. Error bars show SEM. (*D*) Tau RD fibril uptake is temperature-dependent. Tau RD fibrils were added to cells at 150 nM and were incubated at 37 °C or 4 °C for 1 h. (*E*) Tau RD fibril uptake requires ATP. Cells were pretreated at the indicated concentrations of sodium azide and 50 mM deoxyglucose before a 1-h application of 150 nM tau RD fibrils.

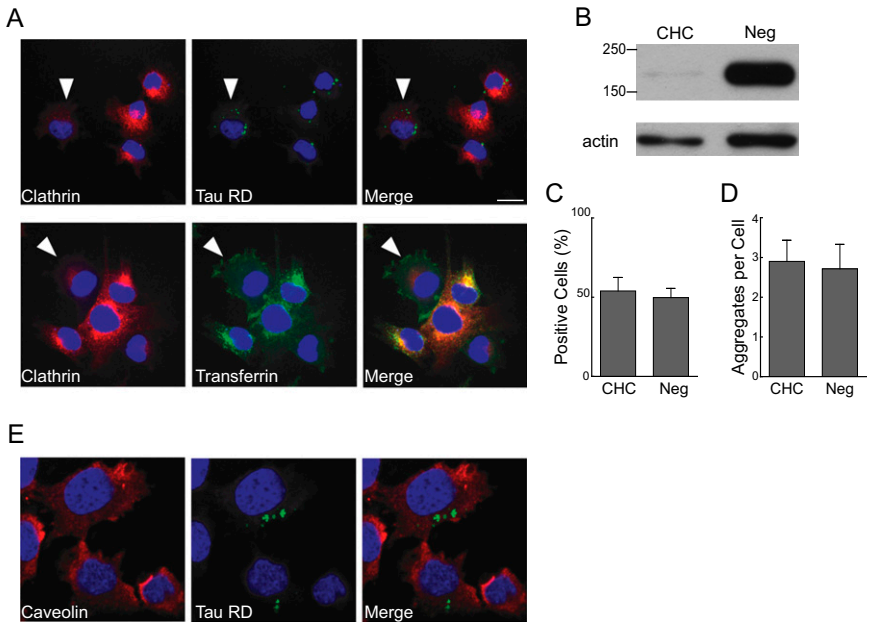

Fig. S2. Tau RD fibril internalization is independent of clathrin- and caveolin-mediated endocytosis. (*A*) CHC is not required for tau RD fibril internalization. C17.2 cells were transfected separately with anti-CHC or AllStars Negative Control siRNA for 24 h and then treated with 150 nM tau RD-488 fibrils (green) or 25 μg/mL Tfn-488 (green) for 1 h. Arrows designate CHC-depleted cells as measured by anti-CHC immunostain (red). (Scale bar: 20 μm.) (*B*) Cells transfected with CHC or negative control siRNA were harvested and immunoblotted with mouse anti-CHC antibody. (*C* and *D*) Cells from *A* were counted and scored for the presence or absence of tau RD aggregates (*C*) and the number of aggregates per cell (*D*). Two hundred cells were counted per experiment, and the graphs represent the average of two independent experiments. Error bars show SEM. (*E*) Cells were treated with 150 nM tau RD-488 fibrils for 1 h, washed with PBS solution, and stained for caveolin-1. No colocalization was observed.

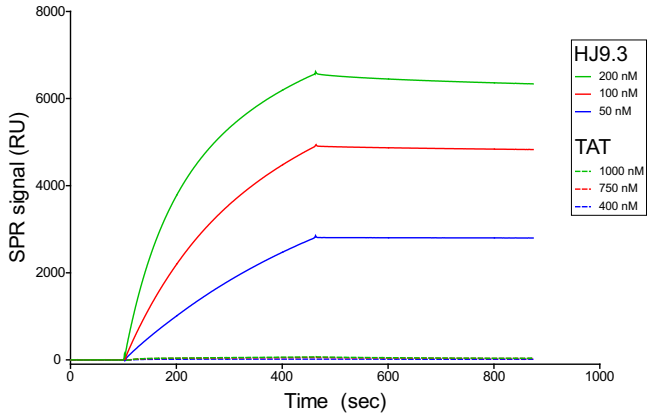

Fig. S3. Overlay of representative SPR sensorgrams resulting from the injection of TAT (dashed lines) or anti-tau antibody HJ9.3 (solid lines) at the indicated concentrations over immobilized tau RD fibrils. RU, resonance units. TAT exhibits no detectable binding to tau RD fibrils.

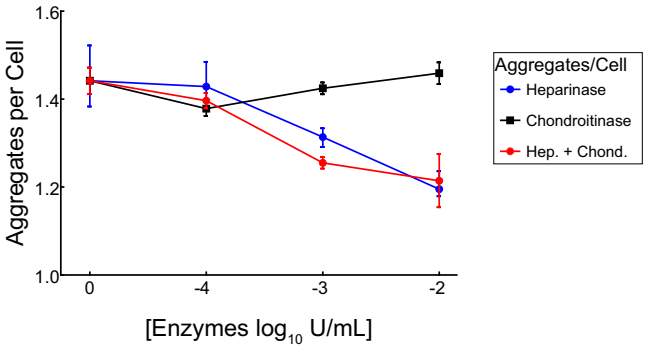

Fig. S4. Average number of aggregates per cell for tau fibril internalization in the presence of heparinase III or chondroitinase AC as measured by automated microscopy analysis. Approximately 40,000 cells were analyzed for each condition, run in duplicate. Error bars show SEM.

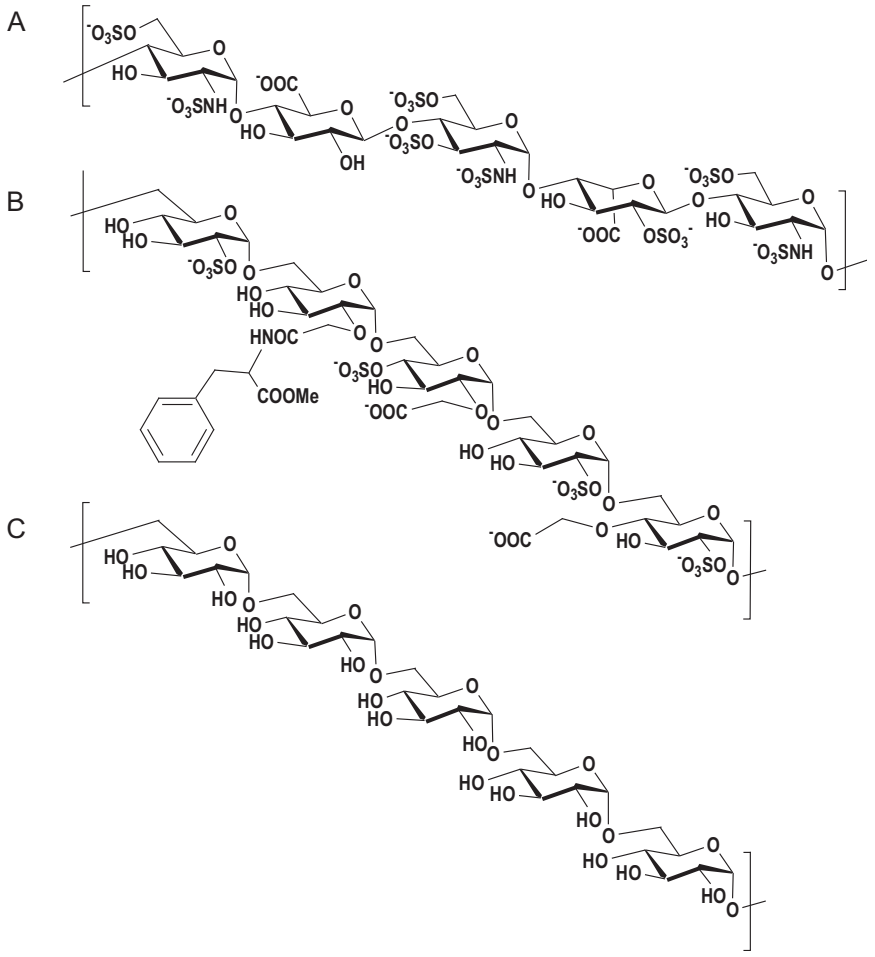

Fig. S5. Schematic structure of heparin, heparin mimetic F6, and polymeric dextran. (*A*) Representative heparin fragment consisting of repeating disaccharide units of D-glucosamine and D-glucuronic acid or L-glucuronic acid. The amounts and distribution of sulfate groups are highly diverse. (*B*) Representative fragment of the heparin mimetic F6 derived from dextran T5 (molecular weight, 5,000 Da). A total of 70% of the F6 glucosidic units contains a sulfate group, 61% a carboxymethyl group, and 15% a phenylalanine methyl ester group. F6 was synthesized, analyzed, and structurally modeled as in the study of Papy-Garcia et al. (1). (*C*) Polymeric dextran.

1. Papy-Garcia D, et al. (2005) Nondegradative sulfation of polysaccharides. Synthesis and structure characterization of biologically active heparan sulfate mimetics. *Macromolecules* 38(11):4647–4654.

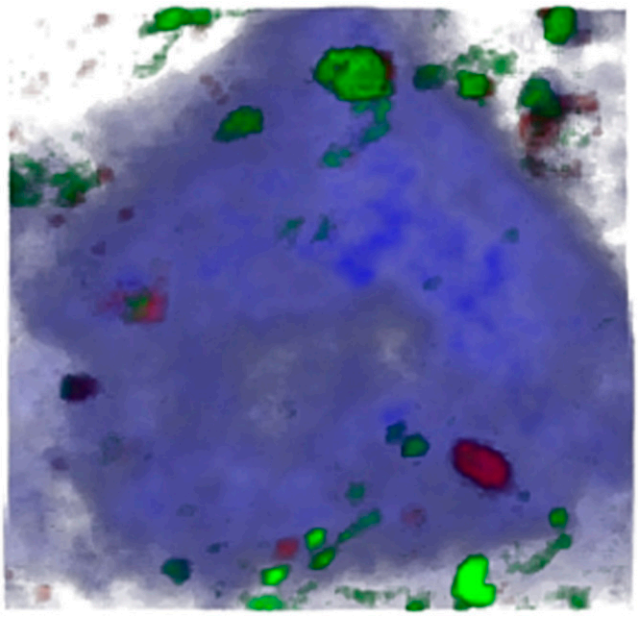

Movie S1. Rotating 3D projection of tau aggregates and transferrin internalized into a neuron. Blue indicates NeuN, red indicates tau aggregates, and green indicates transferrin.

Movie S1